

Electrochemical and Spectroscopic Investigation of Ethanol Oxidation on Au/Pt Nanocomposite

Xingyue Wei*, Xingmin Wang and Lin Zhuo

College of Environment and Resources, Chongqing Technology and Business University, Chongqing 400067, P.R. China

*E-mail: xingyuewei_cq@yeah.net

Received: 28 January 2017 / *Accepted:* 19 February 2017 / *Published:* 12 March 2017

The synthesis of gold/Platinum (Au/Pt) bimetallic nanodendrites was accomplished by a seeded growth method utilizing prefabricated Au nanodendrites as seeds and ascorbic acid as a reductive agent. Through voltammetric characterization, it showed that Au on the step acted as a catalyst for the ethanol oxidation. In order to investigate the effect of Au ratio in the mechanism, FTIR experiments were conducted with the use of normal and isotopically labelled ethanol.

Keywords: Ethanol oxidation; Nanodendrites; Electrochemical study; FTIR; Alkaline direct ethanol fuel cells

1. INTRODUCTION

In recent years, many researchers and experts have been attracted by the controllable synthesis of noble metal nanostructures. This is not only owing to the physiochemical attributes of these nanostructures which are determined by their size and shape [1, 2], but also their broad application range, such as catalysis, electronics, photology, sensor, and nanotechnology [3-5]. Bimetallic nanostructures have attracted much attention due to their excellent attributes in the aspects of catalysis, electronics, photology and magnetism, which are different from monometallic ones to a great extent. Among a variety of bimetallic nanostructures, Pt-based bimetallic nanostructures have been found to have outstanding performance as electrocatalysts in liquid fuel cells. At the same time, they are deemed as a substitution of commercial catalyst [6-10]. Up to now, many efforts have been applied to the synthesis of Pt-based bimetallic nanostructures whose shapes are diverse, like particles[11], tubes [12], cubes [13], nanooctahedra [14], plates [15], as well as nanodendrites [16]. Among these shapes, the nanooctahedra functioning as electrocatalysts have attracted most interest owing to their

large superficial area as well as high specific activity contributed by abundant edges, corners, stepped atoms existing on the branches [16-18].

In the past, a large amount of studies were concentrated on direct alcohol fuel cells that can function as a favourable power source needed for on-board devices as well as portable electronic devices. It is due to the higher energy density and boiling point, and lower toxicity that ethanol is more attractive than methanol. At the same time, it is very easy to produce ethanol in large quantities from farm products or biomass [19, 20]. Nevertheless, activity and durability of electrocatalysts have to be strengthened for the purpose of realizing the commercialization of direct ethanol fuel cells (DEFCs). So far, a large number of researchers have focused on the study of the applications of Pd and Pd-based nanostructures in DEFCs [21]. In contrast, studies with respect to Pt and Pt-based electrocatalysts for ethanol oxidation are very limited, which is likely to be caused by their slow kinetics and low activity on them [22]. Au nanostructures manifested outstanding catalytic activity for the oxidation of CO [23]. Early studies showed that the addition of Au- to Pt-based electrocatalysts has a positive effect on the improvement of catalytic activity and toxin immunity for methanol and formic acid electro-oxidation [24]. Nevertheless, Pt/Au nanostructures which can function as catalysts for ethanol electro-oxidation failed to be reported sufficiently. High catalytic activity of nanodendritic electrocatalysts is attributed to their super great superficial area, as well as lots of activity spots [25]. For instance, Zhu's team made three dendritic Pt nanostructures through sonoelectrochemical way, and the catalytic activity of produced nanodendrites for methanol electro-oxidation was elevated. Han et al. adopted the coreduction method to prepare both dendritic and carbon-supported nanoparticles of Au/Pd alloy, and hydrazine was employed as reductive agent, and the catalytic activity as well as steadiness of the prepared nanodendrites with respect to ethanol electro-oxidation in basic solution was uplifted to a great extent [26-29]. Chen and his colleagues finished the synthesis of Pt/Au and Pt/Pb nanodendrites using hydrothermal means at the temperature of 180 °C, and in this process, the prepared nanodendrites revealed high catalytic activities towards formic acid electro-oxidation [30]. So far, despite the fact that the catalytic activities of nanodendritic electrocatalysts were improved, the synthesis process cannot do without special devices, high temperature and pressure, as well as toxic additives, and so on. The majority of the nanodendritic electrocatalyst reported are monometallic instead of bimetallic, which means that the applications of the latter type in DEFCs are very limited. As a result, there is still a big challenge to figure out an easy and green approach to synthesize bimetallic nanodendritic electrocatalysts for DEFCs. As known by everyone that DEFCs performed in basic solutions cannot only greatly improve the reaction kinetics, but also decrease the rate of catalyst corrosion. Owing to this, it is desirable to adopt the method, namely synthesizing Pt/Au bimetallic nanodendrites for ethanol electro-oxidation in the basic solution to produce economical nanocatalysts for DEFCs with high activity.

This paper is designed to obtain insight into the role Au plays in the ethanol oxidation mechanism with the use of platinum stepped surfaces and FTIR and electrochemical devices. Owing to factors aforementioned, the electrodes are the stepped surfaces with (111) terraces as well as (110) steps. Moreover, the use of isotopically marked ethanol is to trace the reaction mechanism of diverse segments appeared at the time that the C-C bond is disconnected.

2. EXPERIMENTS

2.1. Materials

The source of gold chloride tetrahydrate ($\text{HAuCl}_4 \cdot 4\text{H}_2\text{O}$) as well as ascorbic acid (AA) was Shanghai Chemistry Co., Ltd. (China), while the source of poly diallyl dimethyl ammonium chloride (PDDA, 50 wt% in H_2O , $M_w = 20,000$), Hexachloroplatinic acid (H_2PtCl_6) was Sigma–Aldrich. In addition, Beijing Chemical Factory (Beijing, China) was the source of ethanol ($\text{C}_2\text{H}_5\text{OH}$), vitriol (H_2SO_4), as well as potassium hydroxide (KOH). All chemicals utilized were free from further purification. And double distilled water was employed as the water needed in the experiments (conductivity $\sim 0.0549 \mu\text{s cm}^{-1}$).

2.2. Synthesis of Au/Pt bimetallic nanodendrites

With the purpose of developing Au/Pt bimetallic nanodendrites, the Au nanodendrites prepared in advance were employed as seeds. A certain addition of 10 mM H_2PtCl_6 was put in the solution of seeds and the solution was stirred for half hour, and then it remained intact for 12 hours. In the whole process, the temperature was 30 °C. The molar proportion of AA: H_2PtCl_6 was maintained at 5:1 in order to make sure the entire reduction of H_2PtCl_6 . A scanning electron microscope (SEM) equipped with energy dispersive X-ray analyzer (EDX) (FEI XL30 ESEM FEG) was used to characterize the morphology and composition of the products at an accelerating voltage of 15 kV. X-ray diffraction (XRD) analysis was carried out on a D8 ADVANCE Xray diffractometer using Cu (40 kV, 40 mA) radiation.

2.3. Spectroelectrochemical characterization

Implementation of Spectroelectrochemical tests was accomplished with the use of a Nicolet Magna 850 spectrometer attached with a narrow-band MCT finder. There was a rhombic pillar-shaped CaF_2 window whose cant was at 60° in the spectroelectrochemical cell. The IR spectra were obtained by utilizing *p*-polarized light in the resolution of 8 cm^{-1} . Aiming to improve the ratio of signal to noise, there was an addition of 100 interferograms in every spectrum. The depiction of the spectra was realized through the ratio, namely $\log(R_2/R_1)$. Here, R_1 and R_2 refer to reflectance values with respect to the single beam spectra developed at the potentials of both specimens and reference. The record of the specimen spectra was accomplished when continuous potential steps of 50mV in the forward direction was added from 0.1 to 0.9 V. As for negative bands existing in the spectra, they were in accordance with species which have already been developed at the potential of samples, and the concentration elevated. In contrast, positive bands witnessed a decline of species' concentration. Bipolar bands were discovered absorption species existing at both the potential of samples and the reference, and their frequency relies on the potential (Stark effect).

2.4. Ethanol oxidation

In the research of ethanol oxidation, a 0.5 M C₂H₅OH + 0.1 M H₂SO₄ solution was prepared to accommodate the electrode. With the purpose of preventing ethanol adsorption on platinum, the polarization of the electrode was finished at 0.05 V. And then, for every electrode altered by using Au, the voltammetric research of ethanol electrooxidation was taken down within the potential scope of 0.05–0.09 V. Moreover, chronoamperometric research was conducted in every electrode. The curve of current vs. time in the ethanol comprising solutions was taken down for 600 s adding continuous potential steps of 0.050V starting at 0.50 v and ending at 0.80 V in the forward orientation.

3. RESULTS AND DISCUSSION

The approach of easy and quick liquid phase synthesis was employed to finish the preparation of Au nanodendrites. This course was conducted by decreasing HAuCl₄ at indoor temperature inside the PDDA aqueous solution. In this process, the function of PDDA was both stabilizer and shape manipulator. Representative SEM image of the Au specimens can be seen in Figure A. Through the observation of this figure, it can be found that the Au specimens contain hyperbranched nanodendrites whose stem length is around 0.5–1 μm. Besides, there are a couple of branches existing in the hyperbranched nanodendrites which develop radially away from the central spot and there are lots of secondary leaves which grow on each branch's stem. These Au nanodendrites were adopted to serve as seeds in order to prepare the Au/Pt bimetallic nanodendrites (Figure 1B). Through observation, it can be seen clearly that abundant nanodendrites whose morphology is similar to the Au nanodendrites to some extent were prepared in style. The formation of the highly ordered fishbone-like morphology shows that, at this initial reaction stage, the nucleation and formation of dendrites are mainly dominated by oriented anisotropic growth along certain directions, rather than the diffusion-limited aggregation (DLA) of individual particles [31]. Nevertheless, the surface of the Au₃Pt₁ nanodendrites is coarser than that of the Au nanodendrites, which manifests that Pt metal is likely to be deposited on Au nanodendrites' surface.

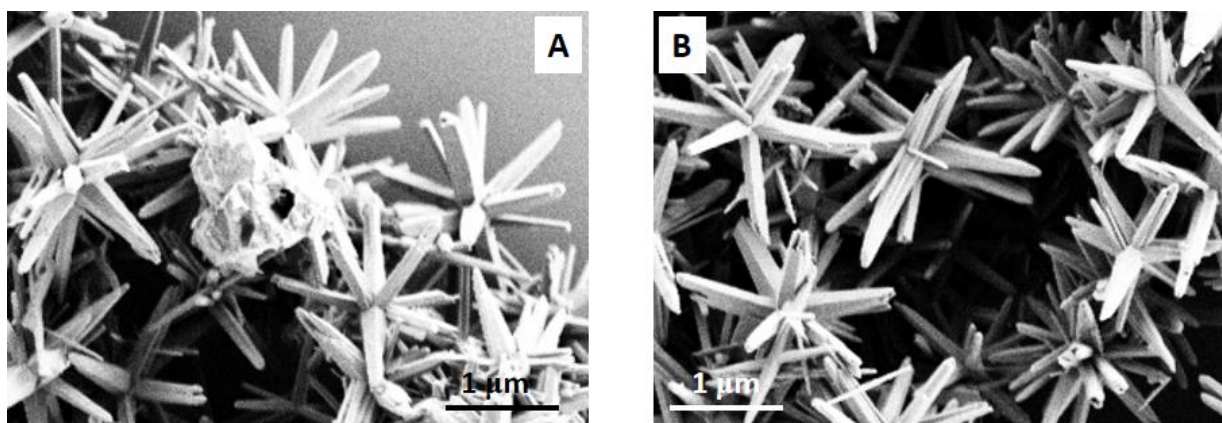


Figure 1. SEM images of the (A) as-prepared Au as well as (B) Au/Pt nanodendrites.

As for the prepared Au_3Pt_1 nanodendrites, their chemical constitution was best revealed by EDX, which could be seen in Figure 2A where the observation of remarkable summits related to Au and Pt was very easy and clear. It indicated that Pt (IV) has already turned into Pt (0) through AA on the Au nanodendrites' external side. What's more, EDX's main peaks were in accordance with Au, indicating that there was likely to have a thin Pt shell or island caused by Au/Pt nanodendrites on the Au nanodendrites.

Figure 2B is the description of the XRD pattern of the specimen. The sites of 5 summits are at 38.1, 44.6, 64.5, 77.5, and 81.6 respectively, which is caused by the (1 1 1), (2 0 0), (2 2 0), (3 1 1), and (2 2 2) planes of face-centered cubic (fcc) Au (JCPDS No. 04-0784), respectively [32, 33]. The alloyed nature of the synthesized PtAu dendrites can be inferred by the following evidence: firstly, there are no distinct reflections characteristic of pure Pt and Au found in the PtAu XRD spectrum; secondary, the peak 2θ values of the PtAu diffraction patterns fall exactly between those of pure Pt and pure Au NPs; Finally, the highly symmetric PtAu reflection peaks can be perfectly fitted with a single analytical function [34, 35].

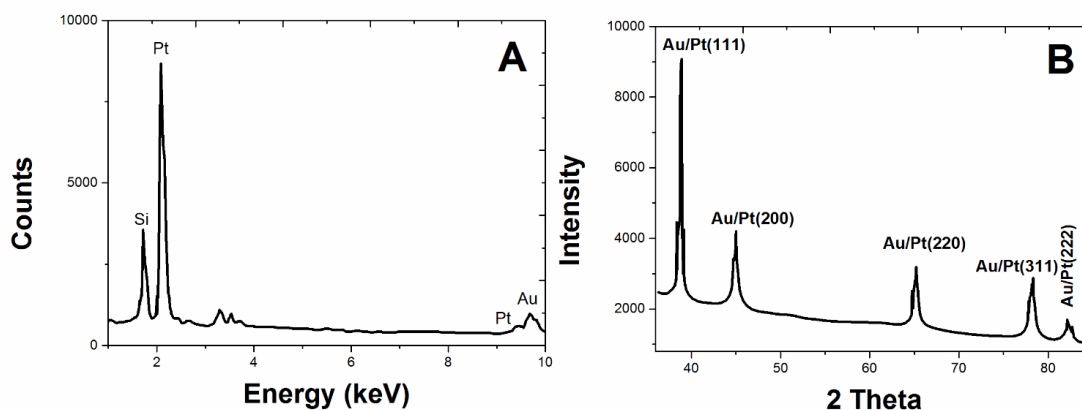


Figure 2. (A) EDX and (B) XRD of the Au/Pt nanodendrites.

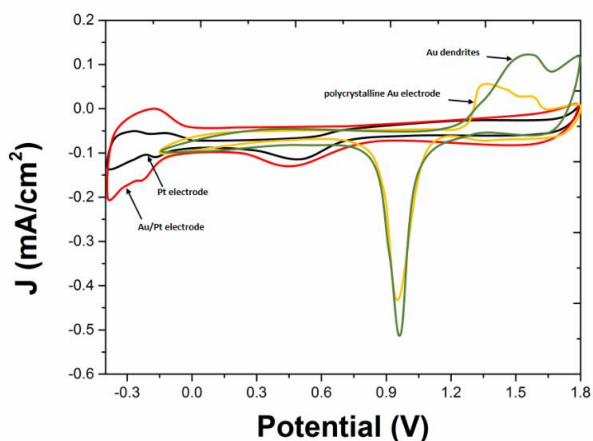


Figure 3. Cyclic voltammograms (CVs) of the pleomorphic Pt electrode, polycrystalline Au electrode, AuPt electrode, as well as Au dendrites electrode in 0.5 M H_2SO_4 solution, scan speed: 50 mV/s.

Electrochemical approach, a good way to depict the superficial atoms, was employed to describe the working electrodes' surface attributes. Figure 3 is the depiction of the CVs of the electrode of polycrystalline Pt (a), Au₃Pt₁ (b), polycrystalline Au (c), as well as Au dendrites (d) in the 0.5 M H₂SO₄ solution, whose scan speed is 50 mV s⁻¹. On the basis of the emergence of hydrogen absorption and desorption summits (from -0.2 to 0.1 V), dual layer charge zones (from 0.1 to 0.3 V), as well as the summits of Pt oxide generation and reduction (from 0.3 to 1.2 V), which are characterized as Pt-based electrode, implied that Pt has deposited on the Au nanodendrites [36]. As for the polycrystalline Pt electrode, Au dendrites electrode, polycrystalline Au electrode as well as Au₃Pt₁ electrode, the values of ECSA were figured out to be 0.013 cm², 0.10 cm², 0.061 cm² and 0.202 cm² respectively. The ECSA is positively related to both the amount of active sites on the electrocatalysts and the catalytic activity in the process of ethanol electro-oxidation.

It was documented that the properties of noble metal nanostructures are determined by a set of physical parameters that include their size, shape, and composition [37]. Our proposed electrode was put in an ethanol-based electrochemical cell for the purpose of investigating the catalytic activity for diverse modified electrodes. The voltammograms which can characterize ethanol oxidation appearing on the modified electrodes can be seen from Figure 4. According to oxidation on the Pt (Figure 4A), the conclusion is made that there is sluggishness between the positive and adverse moving scans. The sluggishness is in connection with the addition of absorption species which function very well, especially CO. These absorption species are developed on the superficial layer of the electrode at low potentials, and they will not leave the surface of the electrode, and only when potentials are higher than 0.6V or 0.7 V, the oxidization of them will occur.

Since there is no this kind of species on the surface when the potential of the scan reaches the peak, the currents on the positive moving scan are relatively low, compared with those of the adverse moving scan. Nevertheless, the currents existing in the positive moving scan reveal the fact that the poison of the surface is caused by itself, so high currents also refer to high tolerance towards poisoning. The positive moving scan for ethanol electrooxidation on both the electrodes of Pt and Pt/Au is observed in Figure 4B. The trend of the currents in the two scans is the same, which means that the modified electrode with the highest currents exists in both scans. What should be emphasized is that there are two well-defined oxidation summits on the positive moving scan at *ca.* 0.46 and 0.69 V. Compared with the peak current densities calculated at 0.46 V, those for the summit are *ca.* 2.4 times greater. It is the variations existing in the ethanol oxidation mechanism that contributed to the appearance of these two different summits, namely the product output's and selectivity's dependence on potential. The currents measured were modified to a large extent owing to the decoration of the step spots with the use of Au. At the time that the adatom coverage in the steps is around 1, the largest currents appear. According to the coverage value, it can be seen that the currents declined significantly. Owing to variations in the step coverage, the recorded currents for ethanol oxidation elevated, and remarkable variations in the aspect of current proportions for the summits at 0.46 and 0.69 V occurred. In the summit at 0.46 V, the intensity is doubled, and its initiation is displaced to potential which are more negative, but at 0.69 V, the summit just changes to more negative potentials in low degree, and no dramatic rise is seen in largest current density. What should be pointed out is that the obvious rise in current for this summit is merely caused by this summit's coverage of the tail

of the summit at 0.46 V, which is positively related with the step coverage. Currents on the surfaces with Pt/Au would decline and change into higher potential. The changes of the voltammetric shape in the positive moving scan are inevitably in connection with variations in the distribution of products for the electrodes.

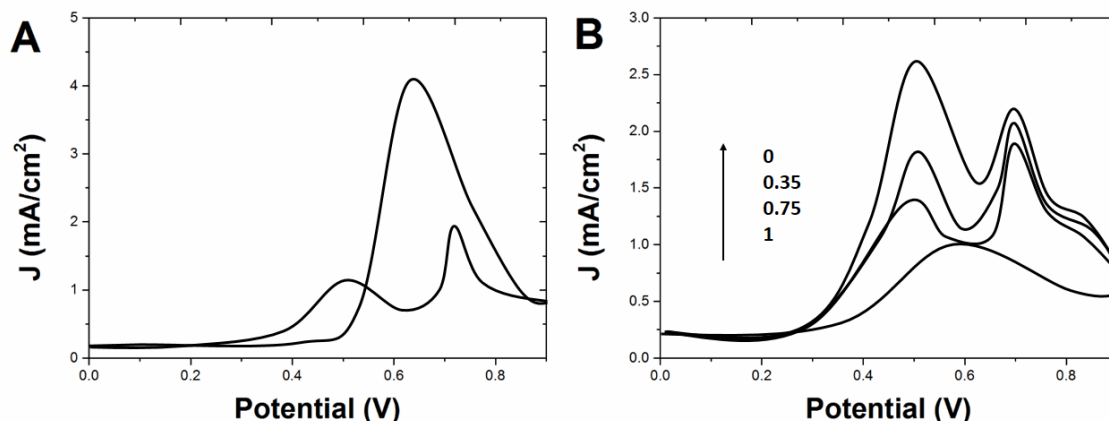


Figure 4. (A) Voltammetric profile for the Pt electrode in 0.5 M C₂H₅OH + 0.1 M H₂SO₄. (B) Positive going scan for the Pt/Au electrode in 0.5 M C₂H₅OH + 0.1 M H₂SO₄ with diverse scan speed: 20 mV/s.

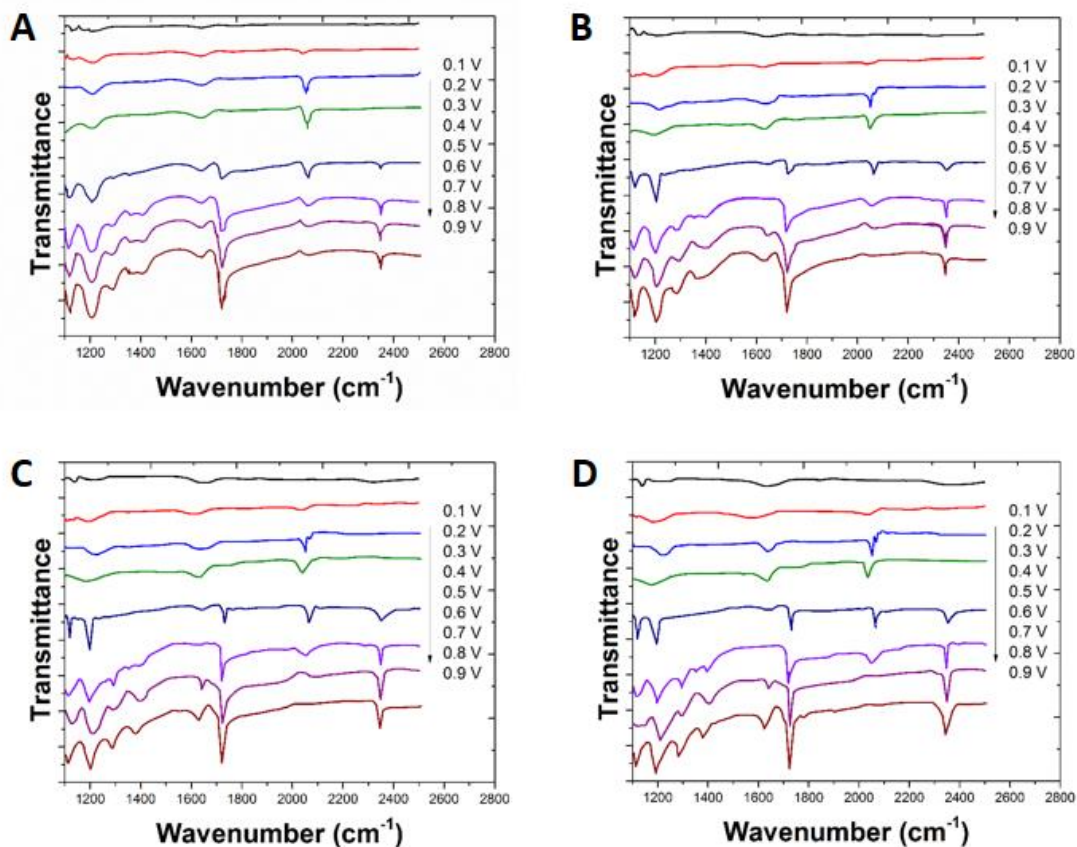


Figure 5. FTIR spectra acquired in 0.5 M C₂H₅OH + 0.1 M H₂SO₄ for the Pt electrode with four diverse ratio of Au. Au ratio: (A) 0.00, (B) 0.35, (C) 0.75 as well as (D) 1.00.

Aiming to study the effect of Au in the mechanism of ethanol oxidation, FTIR tests were conducted on the modified electrodes. These tests can help to define diverse species developed on the surface of the electrode, so as to connect the species with the currents calculated. In the process, the Pt electrode was used and four diverse Pt/Au electrodes were investigated, which were 0.00, 0.35, 0.55 and 1.00 respectively.

Figure 5A depicts Pt electrode's spectra. Through observation, it can be seen clearly that the dissociation of the C-C bond occurs primarily on the step sites existing in the surface of the electrode, so they are regarded as critical sites in the oxidation process to produce CO₂. Owing to the fact that the source of CO₂ is the oxidation of CO adsorbed at potentials higher than 0.6 V, the concentration of CO₂ produced for the electrode is greater as well. The bipolar characteristic of the CO band for potentials over 0.7 V is another vital difference, which is caused by the existence of absorbed CO not only at the specimen potential, but also at the reference one. The existence of steps speeds up the oxidation of CO, so the appearance of CO band when the potentials are high implies that the production of CO is at the speed higher than that of the oxidation. As a result, some CO is still on the surface. In the Pt electrode, such behaviour also existed, which signifies that there is a high activity in this site for the disintegration of the C-C bond.

4. CONCLUSIONS

In a word, the synthesis of Au/Pt bimetallic nanodendrites were accomplished with the application of seeded growth approach utilizing prefabricated Au nanodendrites as seeds and ascorbic acid as a reductive agent. It speeds up the oxidation of CO derived from the disunion of the C-C bond in molecules with the use of a dual-functional mechanism. It only takes effect at the time that on the surface of the platinum, there exist several sites with the capacity to cleave the C-C bond, just as showed in the catalytic action found for the surface of Au.

ACKNOWLEDGEMENT

This work was supported by the open fund of the Key Laboratory of Catalysis Science & Technology of Chongqing Education Commission (No. CQCM-2015-09).

References

1. P. Jain, I. El-Sayed and M. El-Sayed, *Nano Today*, 2 (2007) 18.
2. Y. Xia and N. Halas, *MRS Bulletin*, 30 (2005) 338.
3. M. Daniel and D. Astruc, *Chemical Reviews*, 104 (2004) 293.
4. A. Tao, S. Habas and P. Yang, *Small*, 4 (2008) 310.
5. T. Sau, A. Rogach, F. Jäckel, T. Klar and J. Feldmann, *Adv. Mater.*, 22 (2010) 1805.
6. Z. Yan, Z. Xu, J. Yu and M. Jaroniec, *Appl. Catal. B-Environ.*, 199 (2016) 458.
7. W. Zhang, C. Kong, W. Gao and G. Lu, *Chemical Communications*, 52 (2016) 3038.
8. S. Stevanović, V. Jovanović, J. Rogan and A. Kowal, *Zaštita Materijala*, 57 (2016) 339.
9. Y. Xie, H. Zhang, G. Yao, S.A. Khan, X. Cui, M. Gao and Y. Lin, *Journal of Energy Chemistry*, 26

- (2017) 193.
10. Q. Zhao, Y. Bian, W. Zhang, X. Wang, S. Han and Z. Zeng, *Combustion Science and Technology*, 188 (2016) 306.
 11. Z. Liu, G. Jackson and B. Eichhorn, *Angewandte Chemie International Edition*, 49 (2010) 3173.
 12. D. Pech, M. Brunet, P. Taberna, P. Simon, N. Fabre, F. Mesnilgrete, V. Conédéra and H. Durou, *Journal of Power Sources*, 195 (2010) 1266.
 13. D. Xu, S. Bliznakov, Z. Liu, J. Fang and N. Dimitrov, *Angewandte Chemie*, 122 (2010) 1304.
 14. J. Zhang, H. Yang, J. Fang and S. Zou, *Nano Letters*, 10 (2010) 638.
 15. C. Kuo, T. Hua and M. Huang, *Journal of the American Chemical Society*, 131 (2009) 17871.
 16. S. Guo, S. Dong and E. Wang, *ACS Nano*, 4 (2009) 547.
 17. Q. Shen, L. Jiang, H. Zhang, Q. Min, W. Hou and J.-J. Zhu, *J Phys Chem C*, 112 (2008) 16385.
 18. S. Zhou, K. McIlwrath, G. Jackson and B. Eichhorn, *Journal of the American Chemical Society*, 128 (2006) 1780.
 19. B. Satari, K. Karimi, M.J. Taherzadeh and A. Zamani, *International journal of molecular sciences*, 17 (2016) 302.
 20. S. McIntosh, Z. Zhang, J. Palmer, H. Wong, W. Doherty and T. Vancov, *Biofuels, Bioproducts and Biorefining*, 10 (2016) 346.
 21. C. Bianchini and P. Shen, *Chemical Reviews*, 109 (2009) 4183.
 22. X. Zhang, W. Lu, J. Da, H. Wang, D. Zhao and P.A. Webley, *Chemical Communications*, (2009) 195.
 23. M. Haruta and M. Daté, *Applied Catalysis A: General*, 222 (2001) 427.
 24. X. Gu, X. Cong and Y. Ding, *Chemphyschem : A European Journal of Chemical Physics and Physical Chemistry*, 11 (2010) 841.
 25. X. Wu, P. Anbarasan, H. Neumann and M. Beller, *Angewandte Chemie International Edition*, 49 (2010) 9047.
 26. Y. Lee, M. Kim, Y. Kim, S. Kang, J. Lee and S. Han, *J Phys Chem C*, 114 (2010) 7689.
 27. Z. Liu, R. Zhang, Q. Meng, X. Zhang and Y. Sun, *Medchemcomm*, 7 (2016)
 28. L. Song, C. Kang, Y. Sun, W. Huang, W. Liu and Z. Qian, *Cellular Physiology & Biochemistry International Journal of Experimental Cellular Physiology Biochemistry & Pharmacology*, 40 (2016) 443.
 29. H. Sun, J. Zhu, Y. Chen, Y. Sun, H. Zhi, H. Li and Q. You, *Chinese Journal of Chemistry*, 29 (2011) 1785.
 30. S. Wunderlich and P. Knochel, *Chemical Communications*, (2008) 6387.
 31. J. Wang, D. Thomas and A. Chen, *Chemical Communications*, 40 (2008) 5010.
 32. L. Wang, S. Guo, J. Zhai, X. Hu and S. Dong, *Electrochimica Acta*, 53 (2008) 2776.
 33. D. Joseph and K. Geckeler, *Langmuir*, 25 (2009) 13224.
 34. Y. Song, C. Zhu, H. Li, D. Du and Y. Lin, *Rsc Advances*, 5 (2015) 82617.
 35. X. Han, D. Wang, D. Liu, J. Huang and T. You, *Journal of Colloid & Interface Science*, 367 (2012) 342.
 36. S. Guo, S. Dong and E. Wang, *Energy & Environmental Science*, 3 (2010) 1307.
 37. Y. Jun, J. Lee, J. Choi and J. Cheon, *Journal of Physical Chemistry B*, 109 (2005) 14795.